Cost-efficient and high precision method for the assembly of LN-based photonic crystal slabs on the fiber tip for the implementation of E-field sensors

BRUNO ROBERT, VENANCIO CALERO, MIGUEL-ANGEL SUAREZ, ROLAND SALUT, FLORENT BEHAGUE, FADI BAIDA, NADEGE COURJAL, MARIA-PILAR BERNAL*

FEMTO-ST Institute, University of Bourgogne Franche-Comte, CNRS UMR 6174, Besançon, (France)
**mp.bernal@femto-st.fr*

Abstract: Lab-on-Fiber technology is an emerging topic for sensing cutting-edge technologies due to the high versatility and functionality that it offers when it is combined with different sensitive materials. A particular configuration, which consists of the integration of nanophotonic structures into the tip of a pigtailed fiber, allows the exploitation of light localization performances to produce highly performing sensors. However, integrating such tiny structures into the fiber facet requires complex and expensive procedures. In this work, we report a novel high precision assembly procedure which ensures the parallelism between the photonic chip and the fiber surface, in addition to the alignment with the light injection into the nanostructure. The integrated structure consists of an ultra-compact (19 µm × 19 µm) Photonic Crystal Slab (PCS) structure based on a 700 nm thin film of lithium niobate (LN) which is sensitive to external E-fields via the electro-optic effect. Thus, the assembled sensor detects electric fields, presenting a great linearity and a sensitivity of 170 V/m. This technique shows a way to assemble compact planar nanostructures into fiber facets keeping high throughput, high precision and relatively low costs.

1. Introduction

Optical fibers are experiencing an important growth, in addition to data transport, also in the sensing field due to their unique versatility. They are nowadays employed in applications such as non-invasive medical surgery and structures damage monitoring [1,2]. Moreover, the measurement of other magnitudes such as temperature, refractive index, displacement, pressure and acceleration have been also demonstrated through the so-called Lab-on-Fiber technologies [3]. Recently, the progress in micro- and nanofabrication techniques is making possible the growth of fiber tip sensors whose functional area consist on photonic nanostructures integrated on the fiber extremity such as photonic circuits [4], allowing a new era the of ultra-compact, versatile sensors. Moreover, Guided Resonances (GRs) have been recently implemented on the fiber tip [5,6] due to the coupling efficiency of the fiber propagating mode with the photonic crystal (PhC) mode, in addition to the light localization and vertical confinement performances allowing light-matter interaction enhancement [7,8]. In a recent work from our group [9], a GR-based fiber tip configuration is combined with lithium niobate (LN) in order to enhance its electro- optical performances producing an ultra-compact and distortion-free electric field sensing probe. Thus, a sub-micrometer free standing slab with a photonic crystal (PhC) is designed in a 700 nm TFLN membrane so that it can be integrated on the fiber tip. Despite the fact that the integration of bulk ferroelectric crystals on a fiber tip is a well-known approach [10] producing all-dielectric E-field sensing probes, the fiber tip approach based on the GRs has footprints that are thousands of times smaller than these massive crystal devices. The interest of reduced dimensions is very high since that, in addition to a submillimeter footprint, it offers clear advantages in terms of enhanced linearity with respect to the E-field, micrometer spatial resolution as well as extended bandwidth, only limited by the LN intrinsic bandwidth which is in the order of tens of THz. However, the nanofabrication of LN-based PhC with nanometric precision on LN is still limited to the use of the Focused Ion Beam (FIB) technology [11] or e-beam assisted IBEE techniques [12], which supposes a constraint on the PhC dimensions. Consequently, the mentioned fiber tip E-field sensor [9] utilizes a PhC with an area of 19 µm × 19 µm which requires, due to its compact size, more complex and expensive systems such as the FIB system for the precise welding between the PCS and the fiber facet. This process, due to its serial nature, generally lasts several hours for each sensor head, leading to a low throughput-integration process remaining still far from massive production procedures. As an alternative, transfer-printing techniques based on epoxy solutions have been employed for reducing assembly costs for the welding [13]. However, some constraints remain concerning the parallelism between the fiber and the photonic structure. A promising technique using a camera as feedback loop for the optimization of the angle between both surfaces has been recently reported [14]. Nonetheless, this technique does not take any optical response information as feedback and, as a consequence, the device can only be tested at the end of the assembly. In this paper, we demonstrate a cost-efficient assembly method which simplifies the previously mentioned techniques. Thus, a system based on a stretchable sample holder ensures the parallelism between both surfaces when applying a vertical force, removing the need of complex rotational systems. In addition, an active positioning system is also implemented which allows, by observing the spectrum of the GRs during the assembly, the control of different parameters such as the beam centering. This novel assembly method can be easily used for the batch production of different GR-based fiber tip sensors, for a large range of applications, beyond E-field sensors, like the measurement of physical parameters such as pressure, refractive index, temperature, etc.

2. The stretchable membrane concept

The fiber-tip E-field sensor developed in this work is sketched in Fig. 1(a,b). An optical fiber is pigtailed by a ferrule to obtain a surface wide enough to act as a support for 3mm-diameter photonic chip which represents the sensing part of the device. The chip contains a PhC structure which is designed on a 700nm-thick membrane of X-cut LN centered to the optical fiber core.

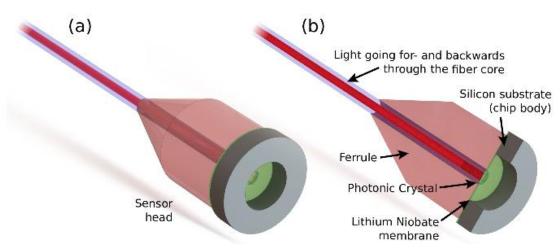

Fig. 1. Rendered images of (a) the fully assembled fibered sensor head and (b) sectional cut.

The membrane is based on a rigid 380µm-thick substrate where only a 250µm-diameter circle located at its center defines the shape of the free-standing membrane. This configuration acts as a protection crown for the PhC whose sensor performances depend on. The PhC geometry study and optimization are beyond the scope of this work but explained in detail in [15]. This thin free-standing PCS can be fabricated from thin film Lithium Niobate-on-insulator (LNOI) wafers, which are nowadays commercially available thanks to ion slicing techniques [16]. The fabrication of the PCS on the LN suspended membrane has been assessed in a recent work [11], demonstrating that highly precise and reproducible spectral performances are achievable. However, the existence of an angle θ between the fiber facet and the PhC plane may produce a serious deterioration of the optical performances, strongly increasing the losses, as demonstrated in [9]. Moreover, the macroscopic size of the ferrule makes even more critical the control of the parallelism since bigger airgaps, between the PCS and the fiber, are introduced when $\theta > 0$, as depicted in Fig. 2(a).

This non-parallelism angle can be minimized to negligible levels by replacing the rigid sample holder by a stretchable membrane. Thus, by applying a force, the membrane is bent, reducing the angle error as shown in Fig. 2(b). The applied force may break the 700nm-thick free-standing membrane. However, the rigid Si-substrate gives enough robustness to the chip to keep its integrity during the process. Once a strong force is applied to the stretchable membrane, both surfaces are forced to $\theta \approx 0$. Then, the epoxy glue can be applied to weld the ferrule and the TFLN which contains the PhC. The applied force on the ferrule towards the chip produces the necessary friction to avoid any displacement of the different elements that can be induced during the epoxy deposition. The epoxy is hardened during 3 hours at room temperature and then the ferrule is pulled back, leading to the assembly sketched in Fig. 2(d). The TFLN is directly in contact with the ferrule surface in order to minimize the air- gap between both surfaces that might lead to Fabry-Perot effect that can deteriorate the spectral performances. As sketched in Fig. 2(d), the chip diameter is slightly higher than the ferrule diameter in order to avoid the epoxy to be deposited on the PhC side. However, issues such as aligning both fiber and PhC centers or ensuring the optimal optical response are not considered in the standalone approach. For this reason, we assist the stretchable membrane approach by an active positioning system as further described.

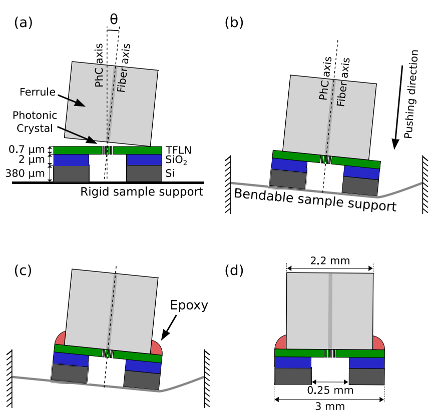

Fig. 2. Assembly of the ferrule-PCS: (a) Fiber approach to the PCS. (b) Pushing the fiber towards the stretchable membrane. (c) Epoxy deposition. (d) Fiber-tips sensor release.

3. The Assembling system

The experimental system which fulfills the mentioned requirements is represented in Fig. 3. The system employs a supercontinuum source which allows a broadband characterization of the transmission spectrum during the assembly. In order to measure the transmitted spectrum, the light is firstly polarized in free space as the photonic crystal structure presents different Fano resonances as function of the incident polarization. Then, the laser is introduced into an inverted microscope which, using an 20x optical objective, injects the light precisely into the PhC structure. The alignment process requires the observation of the laser beam with respect to the PhC surface. For this reason, a VIR/NIS is introduced next to the objective to perform a first coarse alignment. The sample is, as previously described, located on a stretchable membrane.

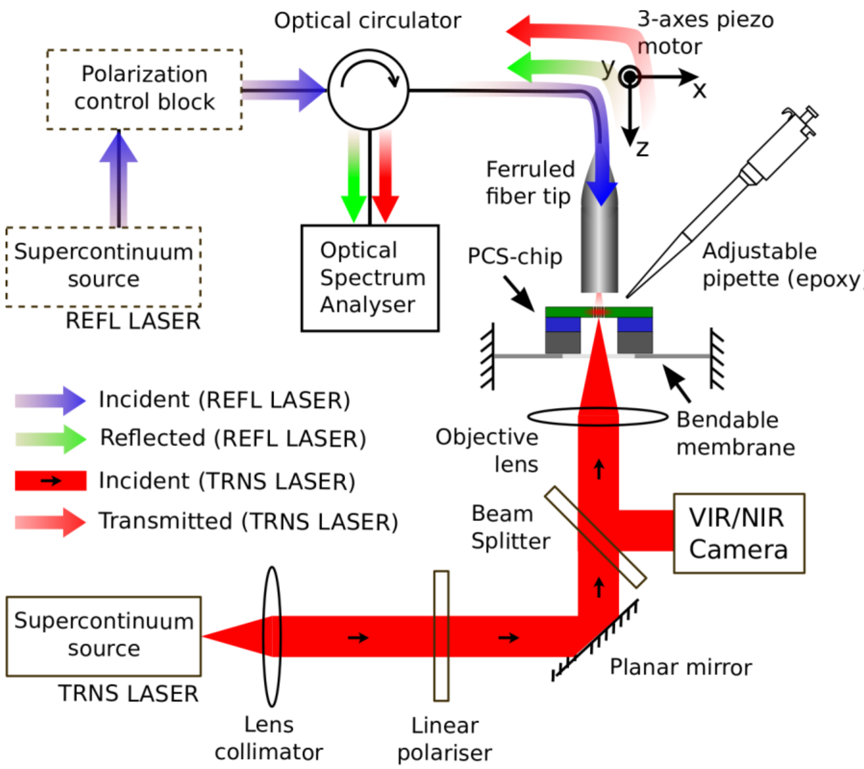

Fig. 3. Experimental system including the dynamic positioning features.

To avoid any perturbation to the microscope observation, the membrane presents a hole at its center. At this point, the ferrule can be approached by employing a 3-axes nano-precision piezoelectric to an approximate distance of 1µm away from the PhC. The ferrule can be firstly aligned by introducing any VIS/NIR light into the fiber, which transmits through the PhC and is captured by the camera. Once aligned, the supercontinuum light is collected by the ferrule and monitored by an Optical Spectrum Analyzer (OSA). The transmission at this distance is shown by the blue curve in Fig. 4(a), which is normalized with respect to the transmitted intensity of the cross polarization

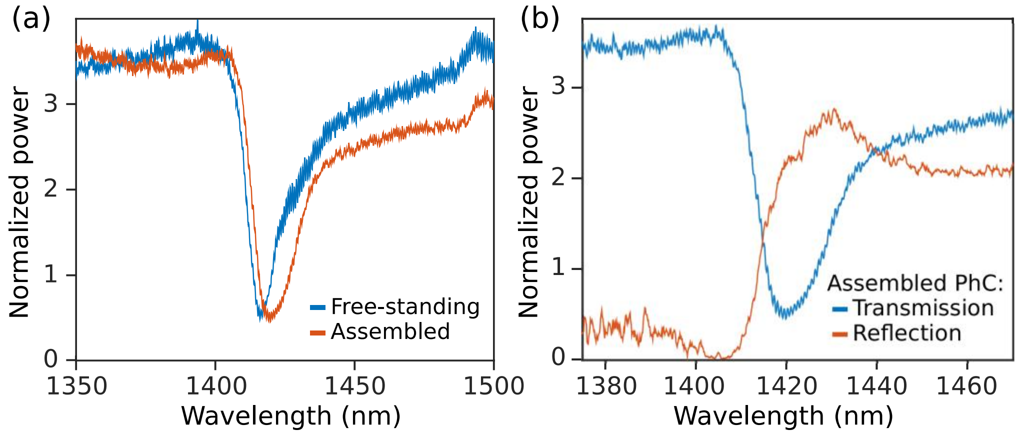

Fig. 4. (a) Normalized transmission spectra for the free-standing PhC (blue) and for the assembled PCS (red). (b) Comparison of both transmission (blue) and reflection (red) of the assembled PCS.

A sub-micrometer precision alignment is performed by optimizing both transmitted power and spectral extinction ratio as a function only of the x and y axes, reducing the degrees of freedom to the translation of x and y. Then, the epoxy is applied with an adjustable pipette. After 1 hour of curing, both trans- mission and reflection spectra are characterized. The resulting transmission spectrum from the assembly, represented by the red curve in Fig. 4(a), reveals that the spectral slope remains above 0.6dB/nm and does not degrade after the assembly. However, a shift of the resonant wavelength of approximately 5 nm is observed between both curves which can be attributed to the correction of the angle θ that changes the light incidence angle into the PhC [17]. In order to obtain the reflection measurement, the supercontinuum source is plugged into the optical circulator. Since the PhC structure is polarization sensitive, the light injected into the ferrule has to be linearly polarized and aligned with the PhC structure. For this reason, a fiber stretching system is installed prior to the optical circulator. A feedback loop for the polarization control can be set by inserting a linear polarization analyzer to the camera, whose axis is aligned with respect to the PhC. The reflection spectrum is represented by the red curve in Fig. 4(b). It can be observed that both curves are complementary.The assembled sensor head is depicted in Fig. 5(a). The photonic chip, the fiber ferrule and the fiber can be clearly distinguished. A SEM picture of the photonic chip, before its assembly onto the ferrule, is shown in Fig. 5(e). As previously described, most of the chip contains the 370μm-thick Si substrate insuring robustness to the sensor head. Despite its circular shape, the chip presents a cut on a side in order to mark the orientation of the PhC and the LN crystallographic axes.

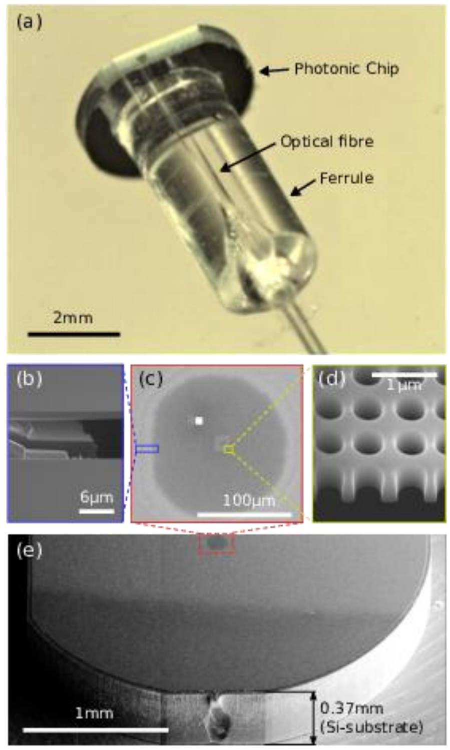

Fig. 5. (a) Assembled sensor. (b) SEM picture of the sectional cut in a border of the membrane. (c) Top view of the free-standing membrane with the PhC structure in the middle. (d) PhC structure on the free-standing membrane. (e) SEM image of the chip with the membrane and the PhC

At the center, the 250 μm-diameter free-standing membrane can be identified due to its darker tone, produced by the lower reflection of the SEM electrons induced by its ultra-thin thickness in comparison with the non-released areas. The membrane is zoomed in Fig. 5(c), where the PhC, whose sectional cut view shown in Fig. 5(d), is located at the center of the membrane. We notice that a bright square can be distinguished which corresponds to a drift-correction mark employed during the FIB fabrication.

4. Electric field sensing measurements

Due to the electro-optic (EO) properties of LN, any applied electric field along the crystallographic Z-axis will induce a linear modification of the refractive index with respect to the electric field. This modification leads to a shift on the resonant frequency of the Fano resonance. Thus, a continuous wave (CW) source has to be employed, whose wavelength is located within the Fano spectral slope. The CW light is then modulated by the applied E-field, whose modulation strength can be optimized by setting the wavelength at the maximum spectral slope of the Fano resonance [11]. In order to evaluate the EO performances, the fibered sensor is approached to a PCB (printed circuit board) containing two coplanar transmission lines where a time-variant periodic signal is applied as depicted in Fig. 6(a). The tunable source wavelength is set at 1576 nm ensuring the optimal EO modulation strength and linearity with respect to the applied E-field [9]. Thus, a time-variant periodic signal is applied on the coplanar lines. During this experiment, the distance between the PC and the electrodes is approximately 600 μm. In addition, the position along the x axis is set to be a at the center of the gap region between the two electrodes since, as determined through electrostatic Finite Element Method (FEM) simulations, the maximum E-field value is located in this region as depicted in Fig. 6(b). The frequency of the introduced signal is set to 178 kHz due to an optimization of crosstalk interferences with other equipment surrounding the system. Moreover, the parameters of the network analyzer have been optimized to minimize the noise floor which has been estimated to be about −132.5 dBm.

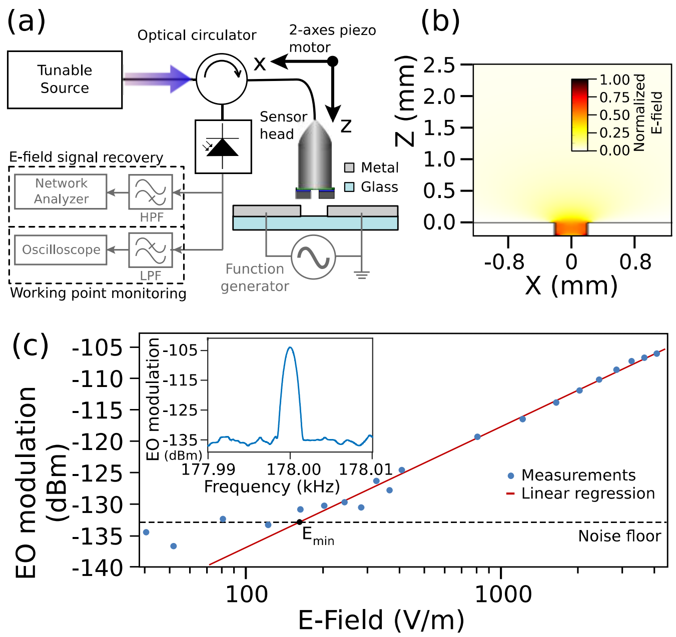

Figure 6: (a) System for the measurement of the E-field sensing. (b) Spatial distribution of the E-field induced by electrodes. (c) Experimental variations of the EO modulation with respect to the applied E-field.

The reflected light, which carries the modulation signal, is introduced in a fast photodiode. The detected signal is split into high and DC signals by using its respective electrical filters. The DC signal carries the information about the reflected power in the absence of any E-field. This is useful since other factors such as a temperature change or deformation of the structure may add a shift of the resonant wavelength, displacing the optimal operation point. Thus, by monitoring the DC signal, the stability of the Fano sensor during its operation can be observed. On the other side, the RF signal carries the E-field information. Thus, the signal is collected in a network analyzer whose measured bandwidth is represented in the inset of Fig. 6(c). The measured modulation frequency (f = 178 kHz) corresponds to the one at the frequency synthesizer and it exhibits an EO modulation strength greater than 30 dB with respect to the noise floor. The linearity of the device as a function of the E-field strength is assessed by varying its value from 40 V/m to 4 kV/m. The resulting EO modulation strength is represented in Fig. 6(b) in function of the applied E-field. A linear regression fit demonstrates a notable linearity, revealing the absence of non-linear effects strong enough to distort the linear operation regime. However, under 250 V/m the regression error increases probably due to the noise. Furthermore, the intersection between the noise floor and the linear regression determines the minimum detectable field whose value is estimated to approximately 170 V/m.

5. Conclusions

We have developed a procedure for the assembly of PhC structures on the tip of an optical fiber. The technique presents several advantages with respect to other solutions. First, the stretching membrane simplifies the alignment procedure and decreases the alignment degrees of freedom from 5 to 2. Secondly, the technique includes dynamic positioning features allowing the observation of the photonic crystal optical response during the x-y axis optimization, allowing a sub-micrometer precision. This solution can be also employed for the integration of LN thin layers, also as well as for a broad range of materials that provide different functions such as temperature, pressure and media sensing. Furthermore, the technique requires relatively inexpensive equipment and may provide high throughput being compatible for batch process for the future industrialization of lab-on-fiber sensors.

Funding. This work was supported by the French Directorate General of Armaments (DGA) (ANR-13- ASTR-0019).

Acknowledgments. We appreciate the technical support of R.-M. Sauvage, L. Robert, S. Bargiel, T. Faure, E. Atie and R. Zegari. We are also grateful to the RENATECH network and the computing center of Franche-Comte.

Disclosures. The author declares no conflicts of interest.

References

1. J.I. Peterson, G.G. Vurek, “Fiber-optic sensors for biomedical applications,” Science **224**, 123-127 (1984).
2. Z. Zhou, J. He, M. Huang, J. He, G. Chen, “Casing pipe damage detection with optical fiber sensors,” Adv. Civil Eng. **9**, 638967 (2010).
3. H. Chikh-Bled, K. Chah, A. Gonzalez-Vila, B. Lasri, C. Caucheteur, “Bahavior of femtosecond laser-induced eccentric fiber Bragg gratings at very high temperatures,” Opt. Lett. **41**, 4048-4051 (2016).
4. D. Taillaert, “Grating couplers as interface optical fibres and nanophotonic waveguides,” PhD dissertation, Guent University (2004).
5. C. Nottbohm, A. Turchanin, A. Beyer, R. Stosch, A. Golzhauser, “Mechanically stacked 1-nm-thick carbon nanosheets, ultrathin layered materials with tunable optical, chemical and electrical properties,” Small **7**, 874-883 (2011).
6. M. Passoni, D. Gerace, L. Carroll, L.C. Andreani, “Grating couplers in silicon-on-insulator: the role of photonic guided resonances on lineshape and bandwidth,” Appl. Phys. Lett. **110**, 041107 (2017).
7. M.L. Brongersma, Y. Lui, S. Fan, “Light management for photovoltaics using high-index nanostructures,” Nature Mater. **13**, 451-460 (2014).
8. J.R. Piper, S. Fan, “Total absorption in a graphene monolayer in the optical regime by critical coupling with a photonic crystal guided resonance,” ACS. Photonics **1**, 347-353 (2014).
9. V. Calero, M.-A. Suarez, R. Salut, A. Caspar, F. Behague, L. Galtier, G. Gaborit, L. Gilette, F. Baida, N. Courjal, M.-P. Bernal, “An ultra-side bandwidth, ultra-high spatial resolution and ultra compact electric field sensor based on Lab-on-fiber technology,” Sci Rep. **9**, 8058 (2019).
10. G. Gaborit, J. Dahdah, F. Lecoche, P. Jarrige, Y. Gaeremynck, E. Duraz, L. Duvillaret, “A nonperturbative electrooptic sensor for in situ electric discharge characterization,” IEEE Trans. Plasma Sci. **41**, 2851- 2857 (2013).
11. V. Calero, M.-A. Suarez, R. Salut, B. Robert, A. Caspar, F. Baida, N. Courjal, M.-P. Bernal, “Towards highly reliable, precise and reproducible fabrication of photonic crystal slabs on lithium niobate,” J. Lightwave Technol. **37**, 698 (2019).
12. R. Geiss, J. Brandt, H. Hartung, A. Thinnermann, T. Pertsch, E.B. Kley, F. Schrempel, “Photonic microstructures in lithium niobate by potassium hydroxide assisted ion beam-enhanced etching,” J. Vac. Sci. Technol. B **33**, 010601 (2015).
13. S. Kim, J. Wu, A. Carlson, S. Jin, A. Kovalsky, P. Glass, Z. Liu, N. Ahmed, S. Elgan, W. Chen, P. Ferreira, M. Sitti, Y. Huang, J. Rogers, “Microstructures eleastomeric surfaces with reversible adhesion and examples of their use in deterministic aseembly by transfer printing,” Proc. Natl. Acad. Sci. U.S.A. **107**, 17095 (2010).
14. A.Kudryavtsev, G.J.Laurent, C.Clevy, B.Tamadarte, P.Lutz, “Analysis of cad model-based visual tracking for microassembly using a new block set for matlab/simulink,” International Journal of Optomechatronics **9**, 295-309 (2015).
15. W. Qiu, A. Ndao, H. Lu, M.-P. Bernal, F. Baida, “Guided resonances on lithium niobate for extremelly small electric field detection investigated by accurate sensitivity analysis,” Opt. Express **24**, 20196-20209 (2016).
16. http://www.nanoln.com
17. L. Chen, Z. Qiang, H. Yang, H. Pang, Z. Ma, W. Zhou, “Polarization and angular dependent transmission on transferred nanomembrane Fano filters,” Opt. Express **17**, 8396-8406 (2009).